P. Sun, A. Rodriguez, W. Kim, X. Huang, C. Fernandez-Pello (2021) *Effect of External and Internal Heating on the Flame Spread and Phase Change of Thin Polyethylene Tubes*, **International Journal of Thermal Sciences**, 107054.
https://doi.org/10.1016/j.ijthermalsci.2021.107054

Effect of External and Internal Heating on the Flame Spread and Phase Change of Thin Polyethylene Tubes

Peiyi Sun[a], Andy Rodriguez[b], Whi Il Kim[b], Xinyan Huang[a,b]*, Carlos Fernandez-Pello[b]

[a] *Research Centre for Fire Safety Engineering, Department of Building Services Engineering, The Hong Kong Polytechnic University, Kowloon, Hong Kong*

[b] *Department of Mechanical Engineering, University of California, Berkeley, CA 94720, USA*

Abstract:

The flame spread over combustible materials is often affected by the fire thermal radiation and convection and the heat exchange with adjacent objects, which are especially complex on melting thermoplastics. This work chooses polyethylene (PE) tubes with a 2-mm thin wall to study the flame-spread behaviors under three heating conditions, (a) hot inner boundary, (b) hot ambient, and (c) external radiation. The tubes could simulate the insulation of electrical wires, and the inner boundary was controlled by flowing oil through at a constant temperature. Results show that just above the fuel molten point, the flame-spread rate unexpectedly decreases with the increasing environmental temperature, because the conductive cooling changed to convective cooling of molten PE. A thin layer of fuel can remain after the flame spread, and as the boundary temperature increases, the remaining PE decreases while the dripping mass increases. Under intense heating, burning behaviors eventually become similar regardless of the heating scenario. This work helps understand the flame spread and phase change of thermoplastic fires, particularly wires and cables, under various heating scenarios of realistic fire events.

Keywords: *Fire spread; Thermoplastic; Wire/cable fire; Melting; Dripping; Cylindrical fuel*

1. Introduction

The spread of flames over the surface of a solid combustible material is often used to determine the material fire hazards and the guidelines for fire suppression [1]. Flame spread is a complex process involving the interaction between the condensed phase (heat transfer, melting, thermal decomposition) and the gas phase (transport, mixing, chemical kinetics) [2,3]. Thus, it depends on the fuel type and chemistry as well as environmental conditions like airflow, pressure, and oxygen concentration [3–5]. In a real fire, the flame spread can also be affected by ambient temperature and the external radiation from the flames and/or hot smoke layer from a nearby fire. In addition, heat and mass transfer in condensed phases can also affect the spread of the flame, especially for thermoplastic fuels with complex phase-change phenomena.

Nomenclature

Symbols

A	cross-section area (mm^2)
Bo	Bond number (-)
c	specific heat (kJ/kg·K)
D	diameter (mm)
g	gravity acceleration (m/s^2)
h	convection coefficent (W/m^2·K)
k	thermal conductivity (W/m·K)
L	heating length (m)
m	mass (g)
Nu	Nusselt number (-)
$\dot{q}''$	heat flux (kW/m^2)
T	temperature (°C)
u	velocity (mm/s)
V_f	flame-spread rate (mm/s)
Y	mass fraction (%)

Greeks

δ	thickness (mm)
μ	dynamic viscosity (Pa·s)
ρ	density (kg/m)
σ	surface tension (Pa)
τ_μ	viscous stress (Pa)
τ_σ	Marangoni surface tension (Pa)

Subscripts

a	ambient
b	burning
c	core/cooling
dr	dripping
ex	extinction
f	flame
g	gas
in	inner boundary
ir	irradiation
m	melting
o	outer/oven
py	pyrolysis
r	remaining
s	surface

Fundamentally, most fire spread is controlled by heat transfer processes [2,3,6]. Many studies have focused on the effect of flame radiation and other external radiation on the flame spread over solid fuel [7–13]. Measuring the flame-spread rate under the external radiation is also a part of the ASTM E-1321-90 standard (also known as LIFT test) to quantify the material fire hazards [14,15]. In general, the rate of flame spread over a solid surface increases with the external heating until the ignition temperature is reached, above which a gas phase premixed type flame propagation occurs [8,9]. A real fire environment with fire irradiation and hot smoke can extend material flammability limit to a lower pressure and oxygen concentration [10–13]. Also, the flame spread can be affected by heat conduction from adjunct objects [16] like the fire in the facade sandwich panel [17]. Similar processes are also often observed in fires of electric wires and cables which are made up of an inner metal core and an external plastic insulation [5,18,19].

The fire spread on thermoplastics becomes more complicated when it involves melting and dripping of the material. Thermoplastic is a group of polymers that have the tendency to melt, such as polyethylene

(PE), polyethylene chloride (PVC), polypropylene (PP), and expanded polystyrene (EPS). Once heated, the solid thermoplastic can melt and the liquid can flow and drip, extending the fire hazards [20–24]. Thus, their fire dynamic differs from both solid and liquid fuels. Thermoplastics are widely used as wire insulation and building façade panels, posing a fire risk [18,25,26]. When the flame spreads over the wire insulation, the heat transfer through the core in the axial direction may become important, especially for a copper or aluminum core [18]. At the same time, the core could act either as a "heat source" or "heat sink," heating or cooling the insulation, respectively. For example, Kobayashi *et al.* [21,27] found that the copper core could act as a "heat source" in the preheating region melting the insulation and accelerating the flame spread, but act as a "heat sink" in the burning region behind the flame front enhancing the burning and reducing the dripping. On the other hand, the wire core, being an excellent thermal conductor, can also be affected by external heating sources. Huang *et al.* [28] showed that the wire core was a "heat sink" to remove the heating from an igniter coil, whereas it was also a "heat source" to enhance the ignition under external radiation [13]. Moreover, the inner Joule heating also contributes to ignition and fire spread, especially under short circuit and overheating [29–32]. Thus, it is important to understand the complex flame spread and phase change (e.g., melting and dripping) for thermoplastic fuels under realistic fire heating scenarios.

In this work, a study is conducted of the effect of three heat transfer mechanisms: internal heating, elevated ambient temperature, and external radiation, on the spread of flames over an insulated wire. This is done by testing the spread of flames over thin-wall PE tubes under these three heating conditions that mimic the real fire scenarios. The internal heating is achieved by flowing hot oil through the tube at a controlled temperature. An oven and radiant lamps are used to control ambient temperature and external radiation separately. The flame-spread rate, as well as the mass fractions of PE burning, dripping, and unburned (or remained), are quantified and discussed using a simplified heat-transfer analysis.

2. Experiment methods

This work aims to study the effect of various heating scenarios on the fire spread over a thin thermoplastic material that simulates the insulation of an electrical wire/cable. The external heating can be viewed as the radiative and convective heat flux from the adjacent flame or hot smoke layer, and the internal heating as the conductive heat flow through the wire core, as illustrated in Fig. 1a. Compared to a flat fuel, an axisymmetric tubular fuel has no edge effect, so both the external heating and internal heating (e.g., Joule heating from the wire core [18,29]) are more uniform, as illustrated in Fig. 1b. Generally, three different heating conditions are most common in fire scenes, (a) internal convection or conduction, (b) external hot environment, and (c) external radiation.

2.1 Thin fuel samples

A typical thin-wall PE tube, which is often used as wire and cable insulation, is selected here to study

the melting and dripping dynamics during the flame spread over insulated wires. The PE sample has a density of 930 kg/m^3 (ρ_p), a low melting point of 105~110 °C (T_m), and a high pyrolysis temperature of about 400 °C (T_{py}), see the TGA analysis in Fig. A1 of the Appendix. To hold the burning PE tube and prevent its bending, a thin-wall (0.18 mm) hollow stainless steel (SS) tube was inserted as the core, as illustrated in Fig. 1b. The combination of the outer PE tube and the inner SS tube has also been used previously as a laboratory wire to study the wire fire behavior [13,28].

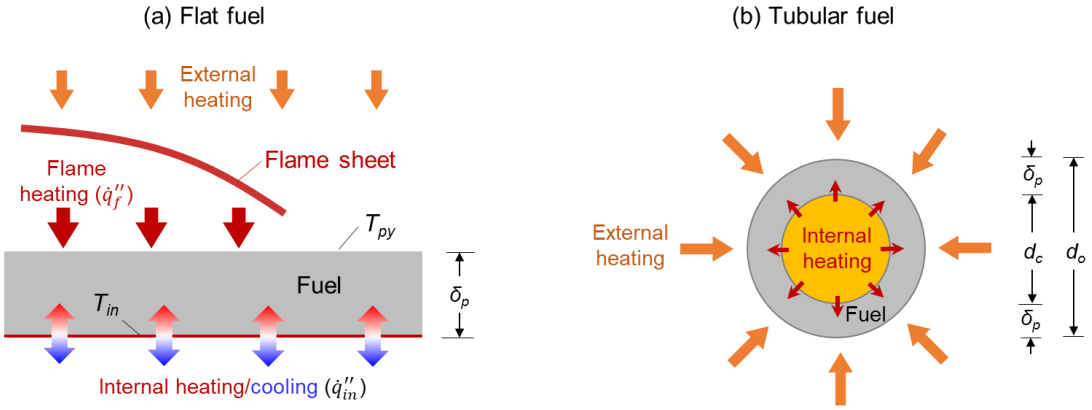

Fig. 1. Diagrams for the external and internal heating of thin fuel: (a) flat fuel and (b) tubular fuel.

Table 1. PE tube configurations: outer diameters (D_o), inner diameter (D_c), thickness (δ_p), and cross-section area ratios (A_c/A_o) [13,21].

Type	D_o (mm)	D_c (mm)	δ_p (mm)	A_c/A_o
1	8.0	3.5	2.25	19% (Cu) 4% (SS)
2	9.0	5.5	1.75	37% (Cu) 5% (SS)

Two sizes of PE tubes were used in the experiments, and their configurations are summarized in Table 1. The thickness of the SS tube (0.18 mm) is much smaller than the inner radius of the PE tube, so that the thermal resistance of the core wall is minimized. The length of the hollow SS tube was 160 mm, longer than that of the PE tube (120 mm), and its end was connected to the sample holder. In addition, the copper (Cu) core was inserted into the PE tube to mimic a wire and study its overall role as “heat source” or “heat sink” under irradiation.

2.2 Internal heating method

The internal heating of the PE tube is produced by flowing a hot vegetable oil of a prescribed constant temperature through the SS-tube core (Fig. 2a). Thus, the resulting heating is a controlled boundary

temperature (T_{in}). The thin-wall SS tube ensures that the inner temperature of the PE tube is basically the same as that of the oil, while minimizes the influence of the heat transfer in the axial direction. The oil flow is driven by a small pump and connected via a high-temperature soft rubber pipe. The oil was stored in a 1-L Pyrex beaker and heated by a hot plate, monitored by a thermocouple (TC 1).

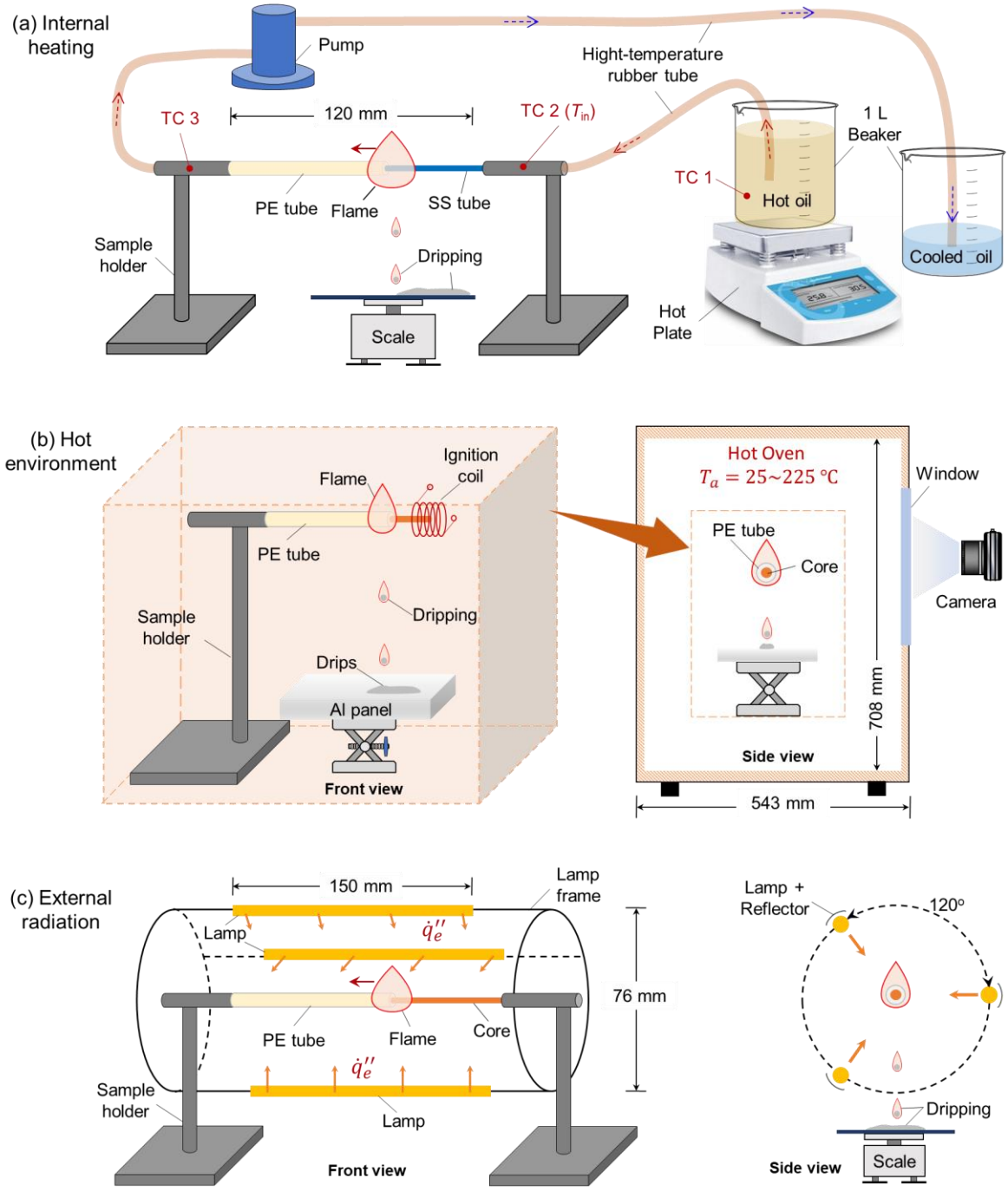

Fig. 2. Diagrams for horizontal flame spread over a PE/SS tube under (a) the internal heating by hot-oil flow, (b) the hot ambient temperature, and (c) the radiant heat flux.

During the internal heating experiment, the oil was first heated slightly above the testing temperature, and then, pumped to the SS tube through connecting pipes. The flow rate was controlled by the power of the pump and fixed to 4 mL/s. The resulting flow speed of the oil was about 50 cm/s for the 3.5-mm SS tube and 20 cm/s for the 5.5-mm SS tube, which was much faster than the rate of flame spread (~1 mm/s). Two thin thermocouples of 0.1-mm thick bead were inserted into the tube to monitor the inlet (TC 2) and outlet (TC 3) temperatures of the oil flow. Compared to the inlet temperature, the outlet temperature was 2-3 ℃ lower before the ignition due to the ambient cooling, while it was 5-10 ℃ higher when there was flame.

The vegetable oil used had a boiling point of about 280 ℃, so the highest flow temperature tested was set to 240 ℃. The lowest flow temperature tested was 0 ℃, when the oil was cooled in an ice bath. After the inlet temperature was stabilized at the prescribed temperature, the PE insulation tube was ignited with a propane flame at the inlet side of the oil so that the direction of flame spread was the same as the direction of the oil flow. If the oil temperature was low, ignition would require a flame heating for 2 min. As the oil temperature was increased, the ignition became easier.

2.3 External heating methods

A hot oven of 180 L was used to simulate the hot environment (e.g., a fire scene), and the whole test setup was placed inside the oven (Fig. 2b). The oven could be set to ambient temperatures ranging from 20 ℃ to 225 ℃, so the overall heating included both convection by the hot air (major heating mode) and radiation from the inner walls (minor). After the oven temperature reached the prescribed value and became stable, the experimental set up containing the PE tube was placed into the oven and then preheated for 3 min. The heating process of PE inside the oven is shown in Fig. A2 of the Appendix. An electric coil was used to ignite the PE tube without opening the oven door. The power of the coil was 70 W, and the ignition lasted for 20 s. There was a window on the oven door that allowed the video capturing for the fire spread.

External radiation is another heating scenario in fire events. In this work, the external heating was generated from three infrared lamps that were equidistantly placed at the 120-degree interval in a cylindrical lamp holder (Fig. 2c). The radiant heaters (Ushio QIH120–500T/S) were quartz infrared halogen lamps with an effective length of 150 mm, fitted into a parabolic strip reflector [13]. Irradiation to the fuel sample was measured by a Schmidt-Boelter radiometer (MEDTHERM Co.). The PE tube sample was placed horizontally on the axis of the test cylinder. The maximum radiation tested in the experiment was set to 11 kW/m^2, which is the critical heat flux for the piloted ignition of PE. In the experiment, the lamps were turned on to preheat the PE for 1 min, and then the propane flame was used to ignite the fuel. With a hollow SS tube core, the ignition was easily achieved after the flame heating for less than 30 s. As the external radiation was increased, the ignition became easier. In addition, a solid copper (Cu) core was applied to further characterize the influence of core material.

2.4 Measurements

To quantify the flame-spread rate, the entire burning progress of the PE tube was recorded with a video camera (Nikon D3200, 30 fps). The flame leading edge and the melting front of the PE were tracked from the video images using a MATLAB code to calculate the flame-spread rate. Both tracking methods provided very similar flame-spread rates, as shown previously [13,21]. At least three repeating tests were conducted for each case to minimize the random errors.

The mass loss fraction is another parameter quantified in this study. Before the experiment, the mass of 12-cm PE sample tube was measured. During the experiment, an analytical scale, with a precision of 1 mg, was placed 10 cm below the fuel to capture the dripping PE. Especially for the hot oven test, the dripping PE fuel was collected by a thick aluminum plate which could quickly cool down the landing drips and extinguish the dripping flame. Finally, the collected dripping mass was measured by the analytical scale to calculate the mass fraction of burning and the dripping fuel. Based on the mass conservation of PE tube, the mass of burnt (m_b) and their mass fractions ($Y_i = m_i/m_0$) can be estimated given the initial mass (m_0), mass of dripping (m_{dr}), and mass of remaining (m_r) [21,33] as

$$m_0 = m_{dr} + m_r + m_b \quad (1a)$$

$$1 = Y_{dr} + Y_r + Y_b \quad (1b)$$

where subscripts dr, r, and b present the dripping, remaining and burning, respectively.

3. Results

3.1. Fire phenomena

After the PE was ignited and the flame spread became relatively stable, the start point of measurement was set as 0 s (Fig. 3), and more details are shown in Supplementary Videos S1-3. The endpoint was set to when the flame leading edge reached the other end of the 12-cm PE tube, so that the average flame-spread rate could be calculated. Once heated, PE tubes became more transparent, as their temperature become closer to the glass transition temperature (see Fig.A3a). Such a color change could be used to track the melting front and the flame inception. Under external radiation, because the lamp illumination was strong, the flame-spread rate was obtained by tracking PE's melting front.

For this PE tube, the flame spread was always accompanied by dripping (see Fig. 3), so that the flame did not burn out the plastic fuel [22,23]. Especially, when the PE tube was burning at a high ambient temperature (200 °C), multiple dripping flows were generated (Fig. 3b and Video S2). When the burning drips landed on the Aluminum board, the dripping flame was quickly quenched. Then, all the dripping mass (m_{dr}) was collected and measured by the electric scale. In addition, there was unburnt PE remaining on the SS tube in the internal heating tests, even under the hottest oil temperature (T_b = 240 °C). This observation

was very different from fire spread test in the base case (no internal and external heating), where all PE tube was burning out in the end, and the remained polymer was negligible (Fig. 3b and c). This is probably due to the oil keeping the PE below its melting point near the SS tube and the PE from burning. After the experiment, the remaining PE (was peeled off from the SS core, and the residual mass (m_r) was measured.

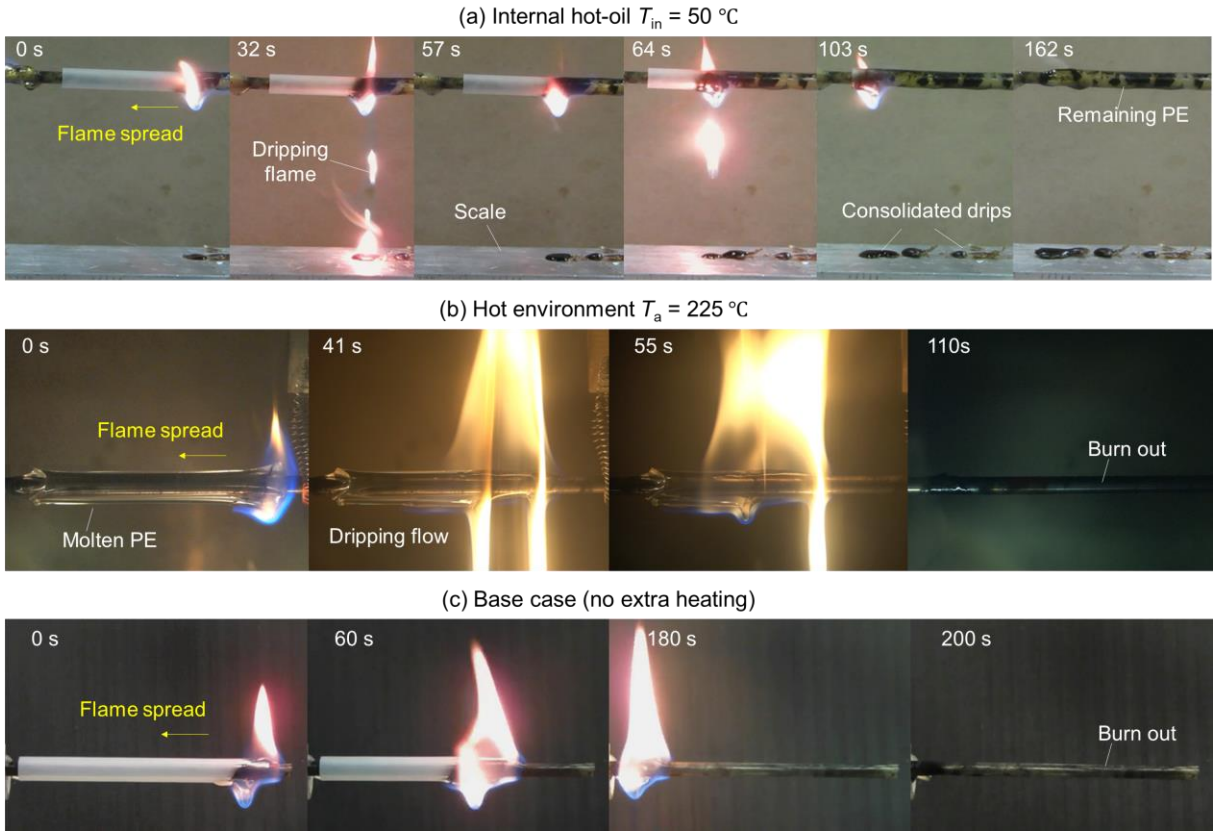

Fig. 3. Snapshots of flame spread over the horizontal 9/5.5-mm PE tube with a hollow SS tube core in the (a) an internal hot-oil flow (T_{in}=50 ℃, Video S1), (b) hot environment (T_a=220 ℃, Video S2), and (c) base case (no extra heating, Video S3).

3.2. Flame-spread rate

Fig. 4 summarizes the flame-spread rate on the PE tubes of two diameters under three heating scenarios, where the flame-spread rate here is an averaged value for the same 10-cm distance under one specific heating condition. For the internal heating test, the boundary condition has been carefully controlled, so the flame spread is almost steady state. For the external heating by the external radiation or the hot ambient, it is difficult to achieve a completely steady-state, because the flame on wire can also affect the environment. Nevertheless, for the hot oven test, although the temperature of the PE tube still increases after ignition, the rate of temperature rise is still quite small, especially for the lower ambient temperature; thus, using the averaged flame-spread rate for the comparison is reasonable (Fig. A2).

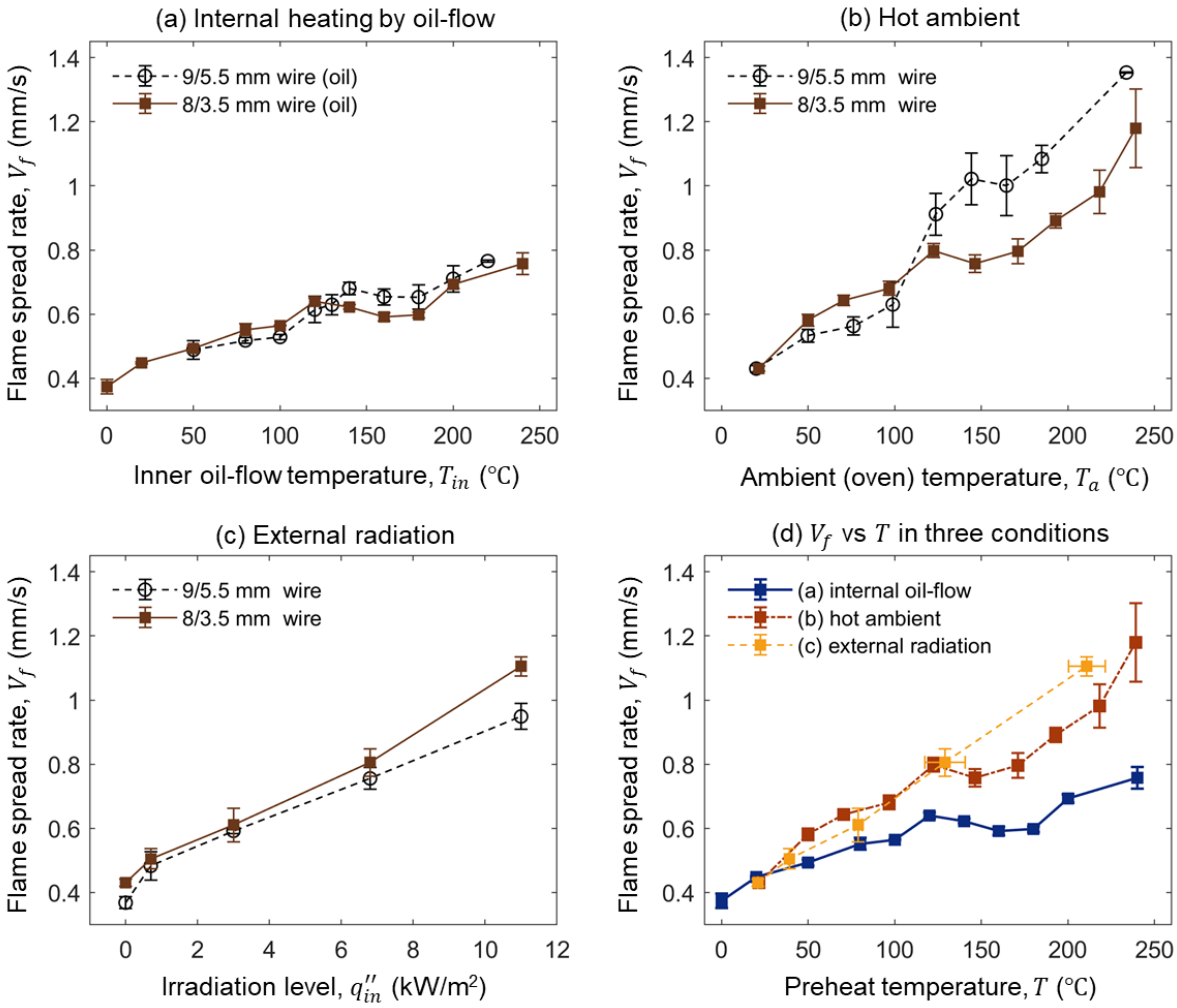

Fig. 4. The rate of flame spread for PE tube with SS core under (a) internal oil-flow, (b) hot environment, (c) external radiation, and (d) the flame-spread rate as the function of temperature for three heating scenarios.

Note that the flame-spread rate was not affected by the dripping process in the burning zone, because the flame spread is mainly controlled by the heat transfer in the preheat zone. Overall, the flame-spread rate is enhanced by any of the three heating scenarios. Moreover, the diameter has no significant effect on the flame-spread rate. For the heating scenario (a) internal heating by controlled inner-boundary, the flame could successfully spread over the 9/5.5-mm PE tube only when the inner oil temperature (T_{in}) was higher than 50 ℃. For 8/3.5 mm tube, the flame could spread even when the oil temperature was reduced to 0 ℃ (Fig. 4a). More importantly, when the inner boundary temperature was in the range of 120 ℃ to 180 ℃, the fire spread rate decreased or remained constant. A similar result was also observed in the heating scenarios of a hot ambient (Fig. 4b) when the ambient temperature increased from 120 ℃ to 180 ℃. This unexpected behavior is a result of an enhanced cooling by the solid thermoplastic melting into liquid (discussed in Section 4.1).

Nevertheless, such an unexpected behavior was not observed under the external radiation, where the flame-spread rate increased monotonically with the irradiation level (Fig. 4c). To link the external radiation with temperature, the surface temperature of the PE tube under certain external radiation was measured right before the ignition. Fig. A2a of the Appendix shows that the PE temperature is increased by irradiation before ignition and after flame spread. Then, the flame-spread rate can be compared as the function of the temperature in three heating scenarios, as summarized in Fig. 4d. Unlike the internal heating and the hot ambient providing a constant preheating temperature to the PE tube, the continuous preheating by the external radiation kept increasing the surface temperature of PE during flame spread, so that the spread rate continued to increase. Therefore, an averaged surface temperature is adopted to represent the preheat temperature under irradiation. For example, the under the irradiation of 11 kW/m^2, the PE surface temperature was measured as 210 ±10 ℃, equivalent to preheating at a hot ambient of T_a = 210 ℃.

In addition, the flame-spread rates on PE tube with Cu core were also measured to investigate the core effects under external radiation (Fig. 5). As the Cu core has a larger heat capacity, it has stronger cooling effects on the PE tube. Then, there would have two ignition results. If applying the flame ignition for 2 min (strong ignition), no PE remained on the Cu core after the flame spread. On the contrary, if only applying the flame ignition for 1 min (weak ignition), a layer of PE would remain on the Cu core. Without external radiation, compared with the thin SS tubular core, the flame spread over PE on the Cu core (strong ignition) is clearly faster than that on the SS core. However, the external radiation weakens the effect of the Cu core on accelerating the flame spread. One probable reason is that Cu has a higher reflectivity, so the overall radiation absorption by PE and Cu core is smaller. The radiation absorption by fuel as found important previously by comparing black and clear PE [34].

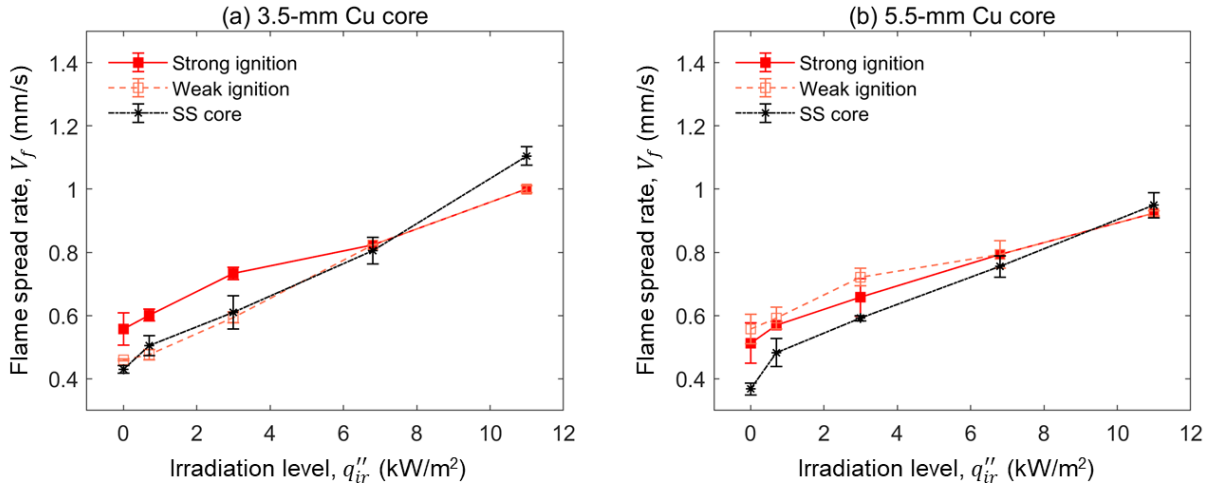

Fig. 5. The flame-spread rate under the external radiation over the horizontal PE tube with (a) 3.5-mm Cu core and (b) 5.5-mm Cu core.

More interestingly, there is a weak-ignition mode for flame spread over PE on Cu core under a low external heat flux ($\dot{q}_e''$< 5 kW/m^2). When the flame ignitor heats the PE, the Cu core acts as a "heat sink" to prevent or prolong the ignition [28]. Therefore, if the ignition is too weak to ignite the entire fuel layer, it is still possible to achieve a flame spread that only involves the outer-layer fuel (δ_m). At the same time, part of PE remains on the Cu core after flame spread like the internal heating case in Fig. 3a. Once raising the irradiation above 5 kW/m^2, no PE will remain on the core, so that only one flame spread model exist.

3.3. Mass loss fractions

Fig. 6 describes the mass loss fraction as a function of oil temperature for the two sizes of PE tubes. Within three repeating tests, the uncertainty of mass fraction is less than 10%, showing a good repeatability. Note that without the internal oil flow, there is no remaining PE ($Y_r = 0$) after the flame spreads over. Clearly, as the inner-boundary temperature increases, more fuel drips, while less fuel remains. The amount of remained PE can be observed by the thickness of the remaining PE, as seen in Fig. 3a. Note that even when the boundary temperature increases to 240 °C, there is about 15% PE left on the SS tube. This indicates that in the burning region (within the flame), the applied hot boundary is still a "heat sink" compared with the pyrolysis temperature ($T_{in} < T_{py}$).

In contrast, without the cooling from the oil flow, the SS tube could be heated by the flame to above 600 °C [21], which is higher than the pyrolysis temperature of PE (~400 °C in Fig. A1). Thus, no fuel would remain on the hot SS tube that is directly heated by the flame. More interestingly, the burning fraction (Y_b) does not change by the inner boundary temperature for the two tube sizes, even though the flame-spread rate doubles when T_{in} increases to 240 °C. As expected, the value of Y_b is also close to the base case without the internal heating flow.

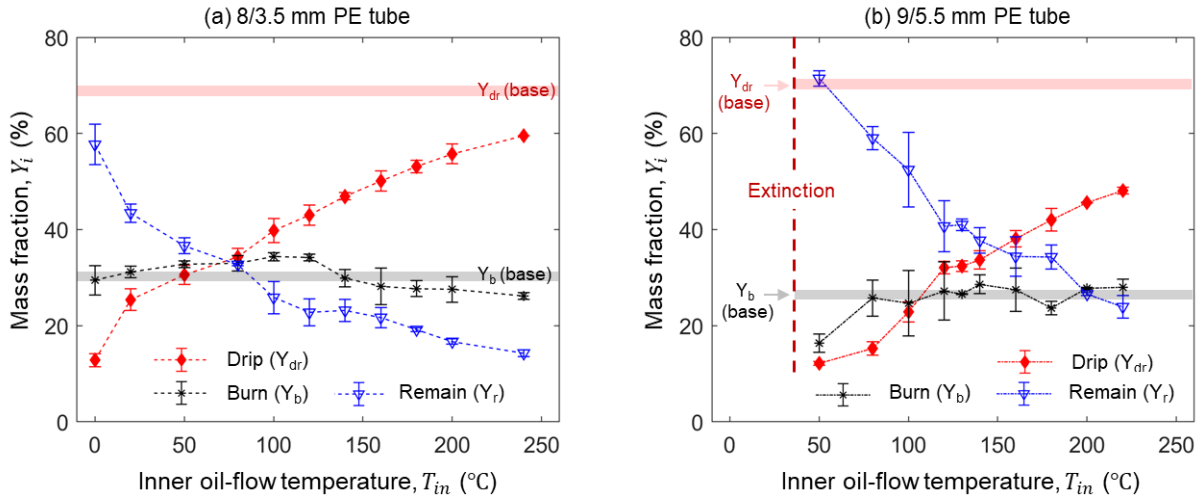

Fig. 6. Mass fractions of dripping (Y_{dr}), burning (Y_b), and remaining (Y_r) in flame spread over the (a) 8/3.5 mm, and (b) 9/5.5-mm horizontal PE tube, with a hollow SS tube core and an inner oil flow.

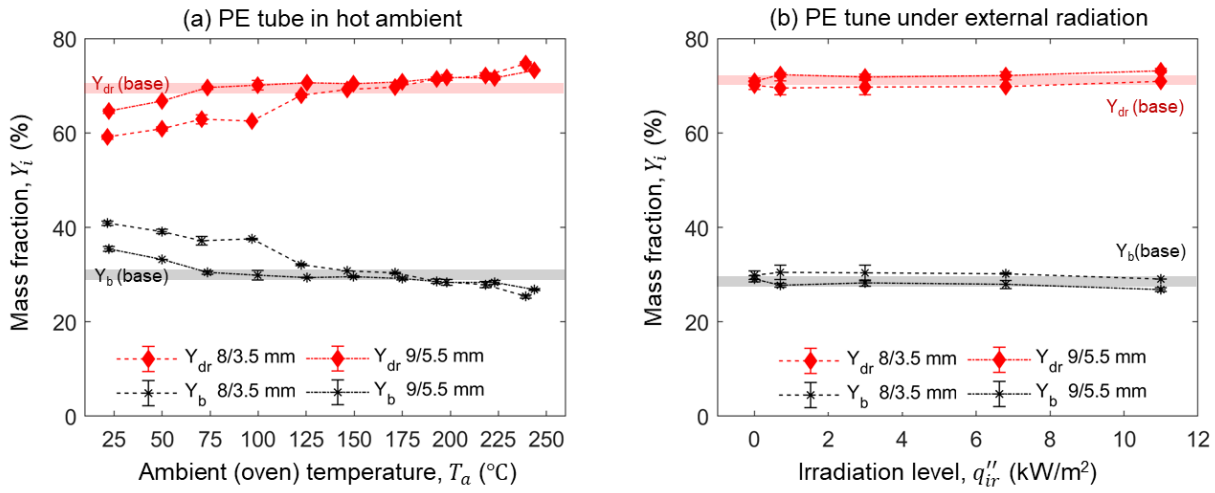

Fig. 7. Mass fractions of dripping (Y_{dr}) and burning (Y_b) in flame spread over the horizontal 8/3.5 mm and 9/5.5 mm PE tube in (a) a hot ambient temperature, and (b) external radiation.

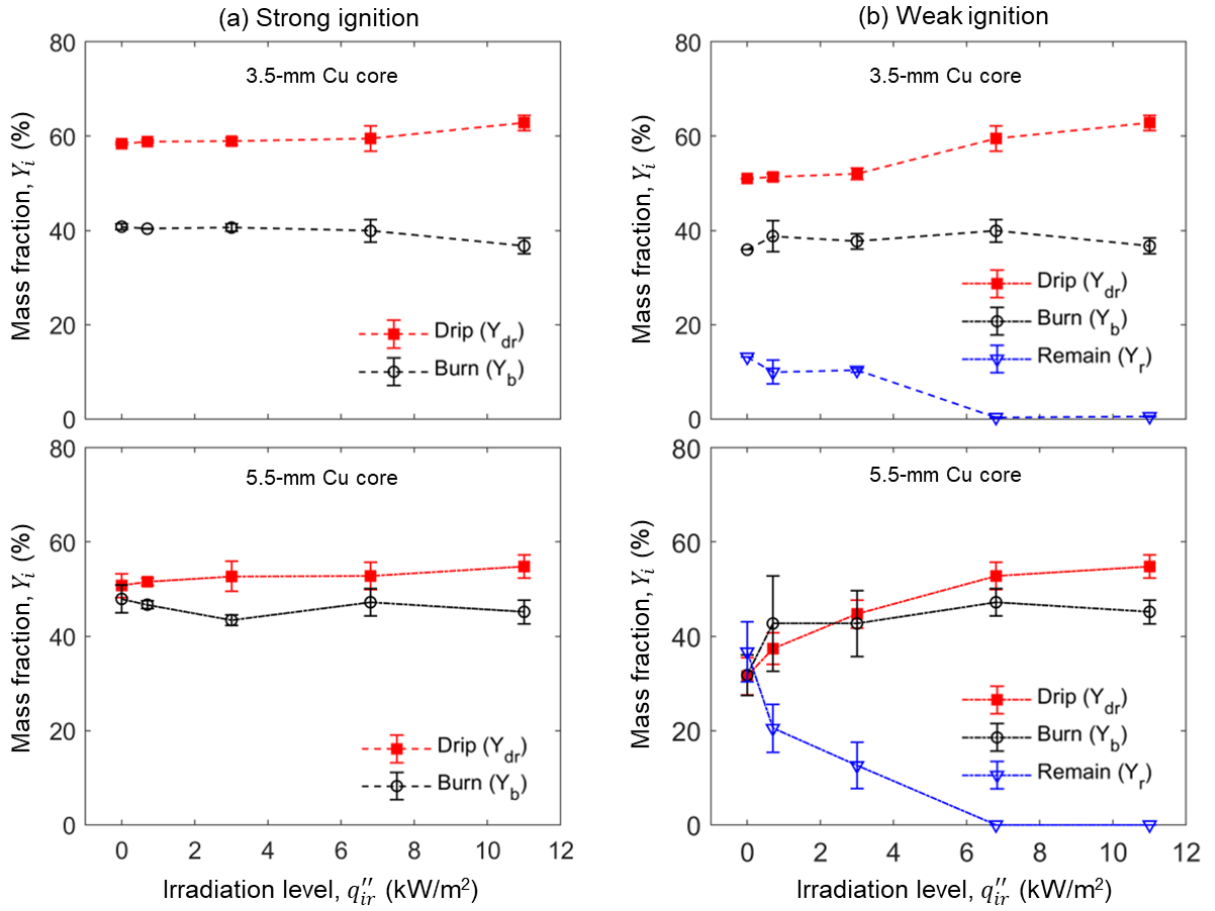

Fig. 8. Mass fractions of PE wires with Cu core under (a) strong ignition, and (b) weak ignition.

Under external heating by either the hot ambient or external radiation, there is no remaining PE after the fire spread. Thus, only two mass fractions are measured: dripping (Y_{dr}) and burning (Y_b). Fig. 7 shows the mass fraction of dripping and burning as a function of ambient temperature and the radiation heat flux separately with two wire diameters. The burning and dripping fractions are almost constant under external radiation (Fig. 7b). Differently, in the hot ambient, the dripping fraction has a clear increase with temperature when the temperature is lower than the melting temperature of PE (~125 °C), but it becomes stable at a hotter ambient. In short, the mass fraction of burning (Y_b) is almost stable, regardless of the heating condition, especially when the PE temperature is higher than the melting point.

Fig. 8 plots the mass fraction of the PE tube with Cu core under external radiation. With a strong ignition, no PE fuel remained on the Cu core. However, with a weak ignition, partial fuel remained when the external radiation is lower than 5 kW/m^2. The diameter of Cu core has a noticeable effect on the mass loss fractions. Generally, when a high-conductance metal is attached to the thermoplastics, the burning and fire-spread behaviors become more complicated. Nevertheless, the mass fraction of burnt fuel is still relatively stable.

4. Discussion

4.1. Effect of phase change on fire spread

A locally reduced fire-spread rate was observed when the inner boundary temperature or the ambient temperature was just above the melting point of PE (Fig. 4a-b). To explain this behavior, a heat-transfer analysis for the flame spread over a thin fuel is applied to the preheating region ahead of the flame front. A schematic of the control volume where the heat transfer analysis is applied is shown in Fig. 9a. The inner boundary temperature of this control volume is well controlled in the internal heating test by the constant oil temperature. The hot flame is clearly the heating source ($\dot{q}_f''$), while the inner boundary is the cooling source ($\dot{q}_b''$) because of $T_{in} < T_p \approx 400$ ℃. Considering that flame spread over a solid is fundamentally a continuous ignition process [2], the fuel has to be preheated to the pyrolysis temperature before ignition. Then, the flame-spread rate (V_f) is expressed qualitatively [15] as

$$V_f \approx \frac{(\dot{q}_f'' - \dot{q}_{in}'')L}{\rho_P c_P \delta_P \Delta T} \sim \frac{\text{Driven Force}}{\text{Thermal Inertia}} \tag{2a}$$

where $\dot{q}''$, ρ, c, and L are heat flux, density, specific heat, and heating length, respectively, and subscripts f, b, and p represent the flame, inner boundary, and polymer. The temperature difference (ΔT) is between the pyrolysis temperature (T_{py}) and the inner boundary temperature (T_b) as

$$\Delta T = T_{py} - T_{in} \tag{3}$$

For all three heating scenarios, T_{in} increases, and ΔT decreases, as the boundary temperature or radiant

flux increases. However, the spread rate does not always increase in a monotonical manner; instead, it decreases when the boundary temperature is between 110 ℃ and 180 ℃ (see Fig. 4).

To explain all these trends, we shall further consider the overall heat flux at the inner boundary ($\dot{q}''_{in}$),

$$\dot{q}''_{in} \approx h_c \Delta T = Nu \frac{k_p}{\delta_p} \Delta T, \qquad \begin{cases} Nu = 1 & (T_{in} \le T_m, \text{conduction}) \\ Nu > 1 & (T_{in} > T_m, \text{convection}) \end{cases} \tag{4}$$

which describes the two-stages cooling effect. If the boundary temperature lower than the molten points, the conductive cooling effect is dominated. Once the temperature exceeds the melting point, the cooling effect transforms into convective cooling. Also illustrated in Fig. 9a, if the boundary temperature increases above the melting point, the cooling effect (i.e., Nu and h_c) is enhanced from conduction to convection as the solid PE layer melts into liquid. Then, the flame-spread rate in Eq. (2a) becomes

$$V_f \approx \frac{L}{\rho_P c_P \delta_P} \left(\frac{\dot{q}''_f}{T_{py} - T_{in}} - h_c \right) \tag{2b}$$

Thus, regarding the flame-spread rate, the "hot" boundary can be either a "heat sink" or a "heat source," depending on the internal cooling (h_c) and the relative magnitudes between T_{in}, T_m, and T_{py}.

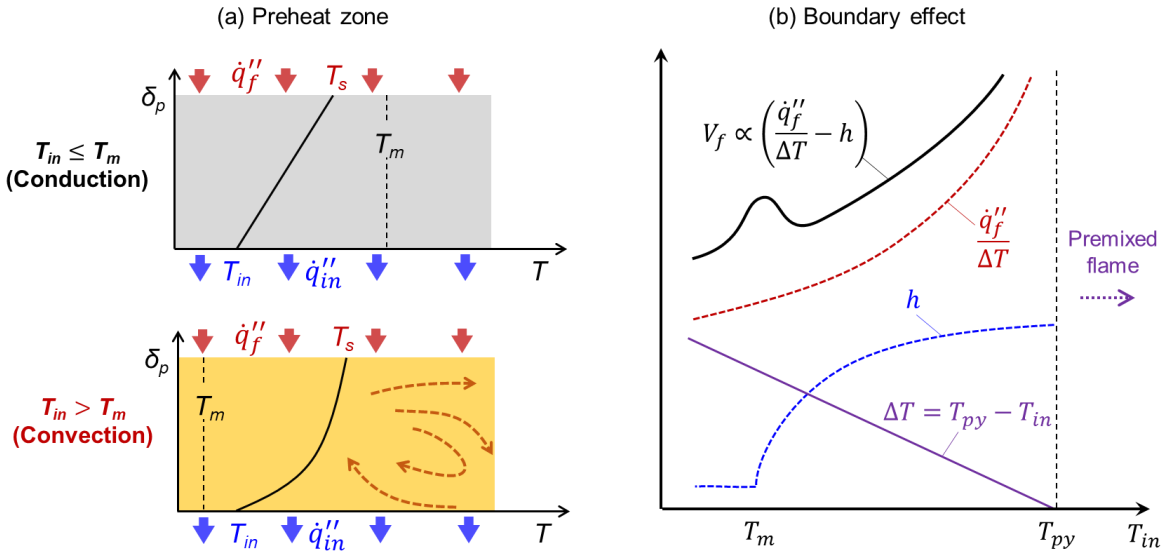

Fig. 9. Illustration of (a) heat transfer in the preheat zone, and (b) effect of inner boundary temperature (T_{in}) on the temperature difference (ΔT), convection coefficient (h), flame heating ($\dot{q}''_f/\Delta T$), and the flame spread (V_f).

Fig. 9b illustrates the dependence of inner-boundary temperature on several key parameters. If $T_{in} < T_m$, the conduction occurs within the solid fuel layer, i.e., $h_c = k_p/\delta_p = \text{const}$. If the inner boundary becomes hot enough to melt the PE ($T_{in} > T_m$), the convection heat transfer occurs, which is evidenced by observed liquid motion. This convection is a combined effect of Marangoni convection (major) and natural

convection (minor). This convective cooling (h_c) increases with temperature, because the viscosity of molten polymer decreases rapidly with the increasing temperature [35]. Although the effective flaming heating, $\dot{q}_f''/(T_{py}-T_{in})$, also increases with T_{in}, its initial rate of increase is smaller than the rapid increase of h_c, because of $T_{in} \ll T_{py}$. Therefore, due to the competition between the effective flaming heating ($\dot{q}_f''/\Delta T$) and the boundary cooling (h_c), the flame-spread rate can decrease locally when the inner-boundary temperature is just above the molten point of fuel (see Fig. 4). Note that this behavior should only occur to with low melting point and low-viscous materials, such as thermoplastics.

Further increasing the inner-boundary temperature, the decrease of $\Delta T = T_{py} - T_{in}$ dominates the flame acceleration. As the inner-boundary temperature is near or higher than the pyrolysis point of the fuel ($\Delta T \to 0$), the flame-spread rate will not go infinite as predicted by Eq. 2(a). Instead, the entire fuel will quickly melt, drip, and pyrolyze; and then, the pyrolysates start to mix with air during the preheating stage. After ignition, the fire spread may become the propagation of a premixed flame, which is a gas-phase phenomenon and similar to flame spread over the liquid fuel above the flashpoint [36]. Although the heat transfer process became more complicated in a hot ambient, test results show that the cooling effect is still enhanced by the phase change process in the preheating zone.

4.2. Distribution of thermoplastic fuel mass

To explain the varied mass fraction of remaining (Y_r) in different heating scenarios, a detailed heat-transfer process within the fuel layer in the burning zone should be considered, as illustrated in Fig. 10. Although the inner temperature (T_{in}) can be higher than PE's molten point, the molten layer near the inner boundary cannot move fast enough compared to the flame-spread rate because of the high viscosity [37].

At the end of the burning zone, the outer surface temperature decreases to the pyrolysis point, and then extinction occurs under a minimum flame heat flux ($\dot{q}_{f,ex}''$). Thus, near extinction, the heat balance satisfies

$$k_p \frac{(T_c - T_{in})}{\delta_r} = h(T_{py} - T_c) = \dot{q}_{f,ex}'' \tag{5}$$

Therefore, after extinction, the mass fraction of the remaining fuel can be estimated as

$$Y_r \approx \frac{\delta_r}{\delta_p} = \frac{k_p(T_c - T_{in})}{\dot{q}_{f,ex}''\delta_P} \tag{6}$$

which decreases with the increasing T_b, as seen in Fig. 6.

Because the heating from the flame is insensitive to the inner-boundary temperature, a constant mass of burning fraction means the residence time of melts (t_r) on the core is almost invariable. This residence time should have three components, (1) the flow time around the core, (2) the accumulation time to a molten ball (drip) below the core, and (3) the constant free-fall time of drip after the detachment.

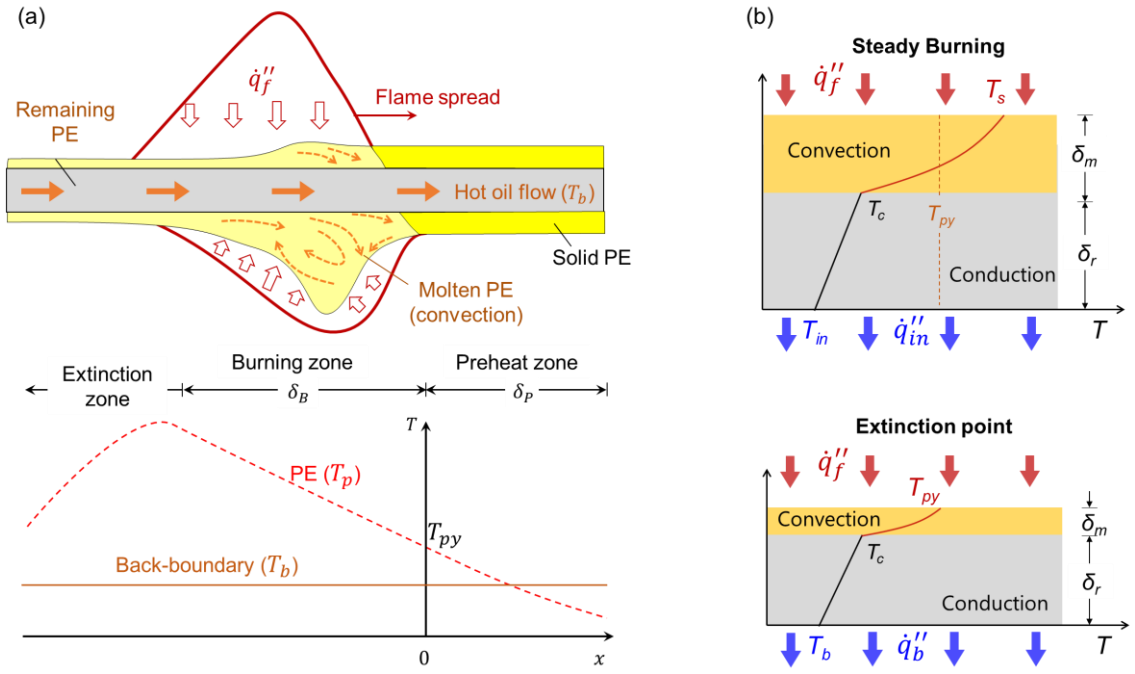

Fig. 10. Illustration of (a) overall heat transfer and temperature profile in different zones, and (b) the heat transfer and temperature profile in fuel for steady burning and near extinction.

The flow time around the core should be controlled by the balance between the resistance of viscous stress (τ_μ) and the drive of Marangoni surface tension (τ_σ) in the axial direction as

$$\tau_\mu = \mu \frac{du}{dr} \approx \mu \frac{u_m}{\delta_m} \tag{7a}$$

$$\tau_\sigma = \frac{\partial \sigma}{\partial T}\frac{\partial T}{\partial D} \approx \left|\frac{\partial \sigma}{\partial T}\right| \frac{T_{in} - T_t}{D} \tag{7b}$$

where the liquid on the bottom is hotter than that on the top, because of a thinner flame-standoff distance on the bottom (Fig. 3). Thus, the liquid moves from bottom to up against gravity. This upward flow was also observed in the experiment via the motion of black residue (soot) which floated on the liquid surface, and such flow velocity (u_m) increases with the thickness of the melting layer, as

$$u_m \approx \left|\frac{\partial \sigma}{\partial T}\right| \frac{(T_{in} - T_t)}{D} \frac{\delta_m}{\mu_m} \tag{8}$$

Therefore, for the accumulation time of the molten ball, the balance between gravity and surface tension becomes important, and controlled by the critical Bond number (or Eötvös number) as

$$Bo = \frac{\rho_p g D^2}{\sigma_m} \tag{9}$$

A similar balance exists for different boundary temperatures, as the measured mass of a single droplet is similar. The viscous effect becomes negligible because the molten ball hangs below the core statically ($u = 0$). Also, because the size of the droplet is relatively small (about 2 mm) [21,38], a thicker moving layer (δ_m) only increases the number of droplets in the same location, but not increases the time of accumulation for each droplet. Therefore, the overall residence time for the molten layer within the flame is similar, resulting in a similar mass fraction of burning.

With various external radiations and different core materials, the mass fraction of burnt fuel is still relatively constant (Fig. 8). There are two possible reasons:

1) For the fuel inside the burning zone, the flame can effectively block the external radiation [39]. In contrast, there is no radiation blockage in the preheat zone, so the external radiation can effectively accelerate the flame spread while not enhance the burning rate.
2) The external radiation is much smaller than the flame heat flux within the flame. The maximum flame heat flux may occur below the tube sample where the flame standoff distance (δ_f) is the smallest.

The flame heating is much larger than the partially blocked external radiation as

$$\dot{q}_f'' \approx k_g \frac{T_f - T_p}{\delta_f} \approx 0.06 \frac{1400 - 400}{0.001} = 60\ \mathrm{kW/m^2} \gg \dot{q}_r'' \qquad (10)$$

Therefore, regardless of the heating scenario, the burning fraction (Y_b) is almost constant, especially when the preheating temperature of PE is higher than its melting point. In other words, in real fire cases, if the temperature excesses the melting temperature of PE, there could be a similar burning behavior in different fire events.

4.3. Influence of the copper core

As shown in Fig. 5, two stable flame-spread modes are observed on the wire with a Cu core, depending on the ignition heat flux. Choosing such a outer layer as the control volume (see Fig. 10), the flame-spread rate of weak ignition may be expressed as

$$V_{f,w\text{-}ig} \approx \frac{(\dot{q}_f'' + \dot{q}_{ir}'' - \dot{q}_{in}'')L}{\rho_P c_P \delta_m \Delta T} \qquad (2c)$$

where $\dot{q}_{ir}''$ is the irradiaton. During the flame spread, the Cu-core boundary still acts as the "heat sink" to cool the inner layer of PE, and the effective fuel thickness is smaller ($\delta_m < \delta_p$).

For a strong ignition, the entire fuel layer is ignited, so that the flame-spread rate may be expressed as

$$V_{f,s\text{-}ig} \approx \frac{(\dot{q}_f'' + \dot{q}_{ir}'' + \dot{q}_{in}'')L}{\rho_P c_P \delta_p \Delta T} \qquad (2d)$$

where the Cu core acts as a heat source in the fuel preheat zone, as observed previously in [21,40]. For a

larger core, the heating effect of the core is usually larger, unless the flame is near the extinction limit [13]. On the other hand, the entire PE layer (δ_p) is involved in the flame spread, so the actual fuel thickness is larger. Therefore, depending on the relative magnitude between $\dot{q}''_f$, $\dot{q}''_{ir}$, and $\dot{q}''_{in}$, as well as that between δ_p and δ_m, the flame-spread rate under a weaker ignition can either be larger or smaller, as seen in Fig. 5. As the irradiation ($\dot{q}''_{ir}$) increases above 5 kW/m^2, the entire PE layer can always be ignited and evolve in the flame spread, so there is only one flame-spread mode. Thus, it is worth noting that the flame-spread phenomena on the plastic insulation of realistic wires and cables are more complex, so does the role of heating and cooling by environment and core material.

5. Concluding remarks

In this work, the flame spread over thin tubular PE fuel is investigated under three possible fire heating scenarios, (a) inner-boundary temperature, (b) hot ambient, and (c) external radiation. The overall flame-spread rate increases when the temperature is increased by three heating scenarios. However, the flame-spread rate decreases when the environmental temperature is just above the melting point of the fuel (120~180 °C). The phase change results in a convective cooling effect, which is more effective in heat loss than conductive cooling.

The PE could remain attached to the core after flame spread if the inner-boundary temperature is below the pyrolysis temperature of fuel. With the boundary temperature increasing, more PE dripped, and less fuel remained. On the other hand, the mass fraction of burning is insensitive to temperature in the three heating scenarios within the tested range. This work helps understand the flame spread and phase-change processes of thin thermoplastic fuels under different heating scenarios in realistic fire events.

CRediT author statement

Peiyi Sun: Investigation, Methodology, Formal analysis. **Andy Rodriguez:** Investigation, Methodology. **Xinyan Huang:** Conceptualization, Methodology, Formal analysis, Supervision, Writing - original draft, Funding acquisition. **Carlos Fernandez-Pello:** Supervision, Writing - Review & Editing, Funding acquisition.

Acknowledgment

XH thanks the support from the National Natural Science Foundation of China (No. 51876183). CFP thanks the support from NASA Grant NNX14AF01G and JAXA (Project “FLARE”). The assistance in experiments from Weiyu He (UC Berkeley) is also acknowledged.

References

[1] Quintiere JG. Fundamental of Fire Phenomena. New York: John Wiley; 2006.

[2] Williams FA. Mechanisms of fire spread. *Symposium (International) on Combustion* 1977;16:1281–94.

[3] Fernandez-Pello AC. The Solid Phase. In: Cox G, editor. Combustion Fundamentals of Fire, San Diego: Academic Press INC.; 1995, p. 31–100.

[4] Ma Y, Zhang X, Lu Y, Lv J, Zhu N, Hu L. Effect of transverse flow on flame spread and extinction over polyethylene-insulated wires. *Proceedings of the Combustion Institute* 2020;000:1–9.

[5] Hu L, Zhu K, Lu Y, Zhang X. An experimental study on flame spread over electrical wire with high conductivity copper core and controlling heat transfer mechanism under sub-atmospheric pressures. *International Journal of Thermal Sciences* 2019;141:141–9.

[6] Williams F a. Urban and wildland fire phenomenology. *Progress in Energy and Combustion Science* 1982;8:317–54.

[7] Bhattacharjee S, Dong K. A numerical investigation of radiation feedback in different regimes of opposed flow flame spread. *International Journal of Heat and Mass Transfer* 2020;150:119358.

[8] Quintiere JG, Harkleroad M, Walton D. Measurement of material flame spread properties. *Combustion Science and Technology* 1983;32:67–89.

[9] Saito K, Williams FA, Wichman IS, Quintiere JG. Upward Turbulent Flame Spread on Wood Under External Radiation. *Journal of Heat Transfer* 1989;111:438.

[10] Osorio AF, Fernandez-pello C, Urban DL, Ruff GA. Limiting conditions for flame spread in fire resistant fabrics. *Proceedings of the Combustion Institute* 2013;34:2691–7.

[11] Osorio AF, Mizutani K, Fernandez-Pello C, Fujita O. Microgravity flammability limits of ETFE insulated wires exposed to external radiation. *Proceedings of the Combustion Institute* 2015;35:2683–9.

[12] Thomsen M, Murphy DC, Fernandez-pello C, Urban DL, Ruff GA. Flame spread limits (LOC) of fire resistant fabrics. *Fire Safety Journal* 2017;91:259–65.

[13] Miyamoto K, Huang X, Hashimoto N, Fujita O, Fernandez-Pello C. Limiting Oxygen Concentration (LOC) of Burning Polyethylene Insulated Wires under External Radiation Limiting Oxygen Concentration (LOC) of Burning Polyethylene Insulated Wires under External Radiation. *Fire Safety Journal* 2016;86:0–17.

[14] ASTM. Standard Method for Determining Material Ignition and Flame Spread Properties. Philadelphia, Pennsylvania: 1990.

[15] Quintiere JG. Fundamentals of fire phenomena. John Wiley; 2006.

[16] Li M, Lu S, Guo J, Wu X, Tsui KL. Effects of pool dimension on flame spread of aviation kerosene coating on a metal substrate. *International Journal of Heat and Mass Transfer* 2015;84:54–60.

[17] Xie Q, Luo S, Da L. Effects of backwall on inner thermal structure in opposed-flow horizontal flame spread of thick PMMA panel. *Applied Thermal Engineering* 2021;185:116424.

[18] Huang X, Nakamura Y. A Review of Fundamental Combustion Phenomena in Wire Fires. *Fire Technology* 2020;56:315–60.

[19] Wang Z, Wang J. Experimental study on flame propagation over horizontal electrical wires under varying pressure. *International Journal of Thermal Sciences* 2020;156:106492.

[20] Xie Q, Tu R, Wang N, Ma X, Jiang X. Experimental study on flowing burning behaviors of a pool fire with dripping of melted thermoplastics. *Journal of Hazardous Materials* 2014;267:48–54.

[21] Kobayashi Y, Huang X, Nakaya S, Tsue M, Fernandez-Pello C. Flame spread over horizontal and vertical wires: The role of dripping and core. *Fire Safety Journal* 2017;91:112–22.

[22] Huang X. Critical Drip Size and Blue Flame Shedding of Dripping Ignition in Fire. *Scientific Reports* 2018;8:16528.

[23] Sun P, Lin S, Huang X. Ignition of thin fuel by thermoplastic drips: An experimental study for the dripping ignition theory. *Fire Safety Journal* 2020:103006.

[24] Kim Y, Hossain A, Nakamura Y. Numerical study of melting of a phase change material (PCM) enhanced by deformation of a liquid-gas interface. *International Journal of Heat and Mass Transfer* 2013;63:101–12.

[25] Bonner M, Rein G. Flammability and multi-objective performance of building façades: Towards optimum design. *International Journal of High-Rise Buildings* 2018;7:363–74.

[26] Srivastava G, Nakrani D, Ghoroi C. Performance of Combustible Facade Systems with Glass, ACP and Firestops in Full-Scale, Real Fire Experiments. *Fire Technology* 2020;56:1575–98.

[27] Kobayashi Y, Konno Y, Huang X, Nakaya S, Tsue M, Hashimoto N, et al. Effect of insulation melting and dripping on opposed flame spread over laboratory simulated electrical wires. *Fire Safety Journal* 2018;95:1–10.

[28] Huang X, Nakamura Y, Williams FA. Ignition-to-spread transition of externally heated electrical wire. *Proceedings of the Combustion Institute* 2013;34:2505–12.

[29] Fujita O, Kyono T, Kido Y, Ito H, Nakamura Y. Ignition of electrical wire insulation with short-term excess electric current in microgravity. *Proceedings of the Combustion Institute* 2011;33:2617–23.

[30] Wang X, He H, Zhao L, Fang J, Wang J, Zhang Y. Ignition and Flame Propagation of Externally Heated Electrical Wires with Electric Currents. *Fire Technology* 2016;52:533–46.

[31] Shimizu K, Kikuchi M, Hashimoto N, Fujita O. A numerical and experimental study of the ignition of insulated electric wire with long-term excess current supply under microgravity. *Proceedings of the Combustion Institute* 2017;36:3063–71.

[32] He H, Zhang Q, Tu R, Zhao L, Liu J, Zhang Y. Molten thermoplastic dripping behavior induced by flame spread over wire insulation under overload currents. *Journal of Hazardous Materials* 2016;320:628–34.

[33] Fang J, Zhang Y, Huang X, Xue Y, Wang J, Zhao S, et al. Dripping and Fire Extinction Limits of Thin Wire: Effect of Pressure and Oxygen. *Combustion Science and Technology* 2021;193:437–52.

[34] Miyamoto K, Huang X, Hashimoto N, Fujita O, Fernandez-pello C. Opposed Flame Spread over Polyethylene Insulated Wires under Varying External Radiations and Oxygen Concentrations. 46th International Conference on Environmental Systems, Vienna, Austria, 10-14 Jul 2016: 2016.

[35] Mendelson RA. Polyethylene Melt Viscosity: Shear Rate-Temperature Superposition. *Journal of Rheology* 1965;9:53.

[36] Drysdale D. An Introduction to Fire Dynamics. 3rd ed. Chichester, UK: John Wiley & Sons, Ltd; 2011.

[37] Van Krevelen DW, Te Nijenhuis K. Properties of Polymers: Their Correlation with Chemical Structure; their Numerical Estimation and Prediction from Additive Group Contributions. Elsevier Science; 2009.

[38] Sun P, Wu C, Zhu F, Wang S, Huang X. Microgravity combustion of polyethylene droplet in drop tower. *Combustion and Flame* 2020;222:18–26.

[39] Jiang F, De Ris JL, Qi H, Khan MM. Radiation blockage in small scale PMMA combustion. *Proceedings of the Combustion Institute* 2011;33:2657–64.

[40] Nakamura Y, Yoshimura N, Ito H, Azumaya K, Fujita O. Flame spread over electric wire in sub-atmospheric pressure. *Proceedings of the Combustion Institute* 2009;32 II:2559–66.

Appendix

The thermogravimetric analysis (TGA) analysis of PE sample was conducted with a PerkinElmer STA 6000 Simultaneous Thermal Analyser. The initial mass of PE sample was 3-5 mg, and samples were heated at the constant rates of 20 and 50 K/min. Two oxygen concentrations were selected, 0% (nitrogen) and 21% (air), with a flow rate of 50 mL/min. Experiments were repeated twice for each case, and good repeatability is shown. Fig. A1 shows the mass-loss rate curves of the PE insulation sample. In general, the decomposition temperature increases with the heating rate, while decreases in an oxidative atmosphere. Previous measurements showed that the heating rate of PE by flame was about 50-200 K/min [21], so that it is expected that the decomposition of PE within the flame (i.e., without oxygen) occurs above 400 ℃.

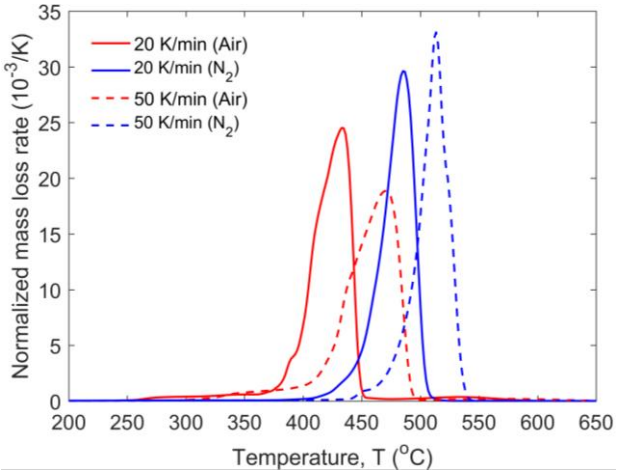

Fig. A1. Mass-loss rate in the thermogravimetric analysis (TGA) of the PE in both air and nitrogen.

In the experiment, wires were preheated before ignition. Then, the evolution of surface temperature was recorded as a function of time. Fig. A2a plots the temperature increasing process under the external radiation with 3 kW/m^2 and 11 kW/m^2 heat flux separately. Obviously, the heating rate is larger for the wire under a higher heat flux. However, the larger heat flux also means it will take a longer time to reach the steady state. Specifically, the preheating time is only 1 min in external radiation test. Thus, the temperature was continually increased and quickly exceeded 165 ℃ after the preheating stage for the wire under 11 kW/m^2 radiation. Differently, in the hot oven test, the surface temperature is always lower than the ambient temperature, as shown in Fig. A2b. After 3 mins preheating time, the surface temperature of wire is relatively stable especially for wires in a lower temperature.

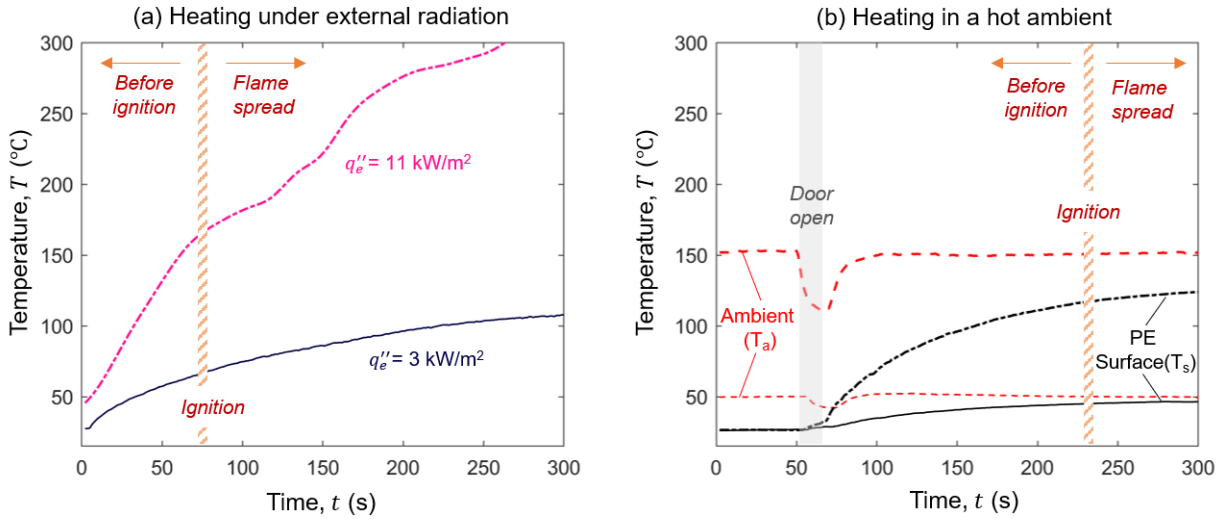

Fig. A2. Temperature propagation of 8/3.5 mm PE tube with SS core under (a) external radiations of 3 kW/m^2 and 11 kW/m^2 and (b) the oven temperature of 50 °C and 150 °C.

Fig.A3a shows the color changing of the PE tube during flame spread. When the temperature of PE solid exceeds its glass transition temperature, it becomes transparent. We can clearly observe the melting edge, and the front of the blue flame. The FSR can be measured by tracking the position of the flame front or melting edge. Fig.A3b plots the position of the flame front and melting edge for a tube in hot ambient temperature (50 °C). Essentially, the flame front is at the same position with the melting front.

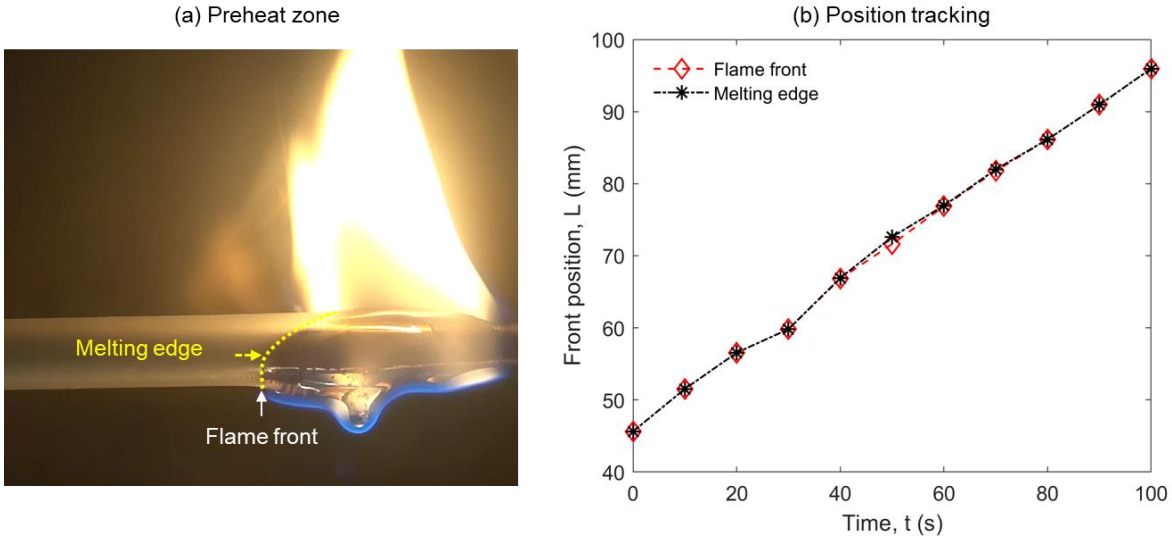

Fig. A3. The photograph shows the partial transparent PE tube during burning and (b) the positions of the melting edge and flame front for the PE tube burning in a hot ambient (50 °C).